# Computational Modeling of Gas/Particle Flow in a Riser

**Arild Samuelsberg and Bjørn H. Hjertager**
Telemark Technological R&D Centre (Tel-Tek) and Telemark Institute of Technology (HiT-TF), N-3914 Porsgrunn, Norway

*Axial solid velocity, solid volume fraction, and solid shear viscosity were computed in the riser of a circulating fluidized-bed reactor using a two-phase 2-D computational fluid dynamic model. The time-averaged model predictions agree well with the experimental data of Miller and Gidaspow (1992). The model predicts a core-annulus flow in the riser, similar to that found experimentally. The maximum velocity in the core agrees well with the measurements, but the downflow in the annulus is somewhat overpredicted. The solid volume fractions profiles agree well in both core and annulus, with discrepancy in the core at the level close to the inlet. The radial profile of solid shear viscosity computed by the turbulent kinetic energy model is ten times lower in the core than that found experimentally, but with a linear function of solid volume fraction in the measurement, the computed profile agrees well with experiments.*

## Introduction

Flow processes and performance of industrial chemical multiphase reactors very often depend on the geometrical design. In order to ensure and predict optimum behavior of reactors, a simulation tool should be capable of coupling a mathematical reactor model to the geometrical layout.

Despite huge economical investments needed to build new or optimize existing reactors, very little is known about the fluid dynamic behavior of multiphase reactors. No reliable simulation tools are available to describe the influences of complex geometries, multiple gas inlets, chemical reaction, internal backmixing, and heat transfer on the flow pattern. Several models for describing the hydrodynamics of fluidized-bed reactors have been published during the last 30 years. These models can be classified into three broad groups (Harris and Davidson, 1993). The first group involves models that predict the axial distribution of the solid phase, but not the radial variation of solids. The second includes models that divide the flow into two or more distinct regions. The third comprises models which are based on numerical modeling of the conservation equations for mass, momentum, and energy for both phases. Such models give the axial and radial variation of the velocity components, chemical species, enthalpy, and volume fraction of the phases involved.

### *Previous work*

In the late 1970s, the development and availability of new high speed computers and new computational techniques made it possible to solve the basic Navier-Stokes equation numerically. Gidaspow (1986) reviewed three different codes that were based on modeling of the basic conservation equations for mass, momentum, and energy for gas solid flow. The models differed in formulation of the conservation equations and computational techniques, but all were inviscid. Nevertheless, these numerical models were able to simulate and predict realistic processes occurring in bubbling fluidized beds. Several groups later extended the models using the basic principles developed to study various processes in bubbling fluidized-bed reactors, for instance: erosion (Lyczkowski et al., 1989; Ding and Lyczkowski, 1992); chemical reaction and heat transfer (Kostamis et al., 1987; Kuipers, 1990; Theologos and Markatos, 1992, 1993; Samuelsberg and Hjertager, 1995) and bubbles and porosities (Ding and Gidaspow, 1990; Kuipers et al., 1992a,b). Based on extensions of the same models used in bubbling fluidized-bed reactors, core annulus flow and cluster formation have been simulated. To be able to simulate these features, the most important extension of the models was to incorporate gas and solid viscosities. Solids viscosity can be incorporated by using an ef-

fective constant viscosity, or it can be computed from a relevant turbulence model. Gidaspow et al. (1989) were the first to publish computed core annulus flow and cluster formation in a riser. Tsuo and Gidaspow (1990) and Samuelsberg and Hjertager (1996) continued this work.

### *Turbulence modeling in gas solid flow*

Two different approaches have been used in turbulence modeling in gas solid flow. The first is using the conservation of mass and momentum equations described using an Eulerian approach and an extension in single phase flows of the well-known $k$-$\epsilon$ model in the carrier phase to predict the effect of the dispersed phase. In these models, particle-particle interactions in the solid phase are neglected. This limitation makes these models unsuitable for modeling of bubbling beds, pneumatic transport, and riser reactors. The second approach of turbulence modeling used in gas-solid flow is based on kinetic theories of nonuniform dense gases as presented in Chapman and Cowling (1970). The first to derive and solve a conservation equation for the so-called granular temperature was Jenkins and Savage (1983). Their calculations were based on a Maxwellian velocity distribution and considered only the collisional transport of momentum and granular temperature. As an illustration of this model, they considered the shear flow between two parallel plates in relative motion. Lun et al. (1984) continued this work and considered the kinetic and collisional transport for a monosized sample of nearly inelastic spheres with a correction to the Maxwellian velocity distribution.

None of the models mentioned above considered the interstitial fluid, and the solid phase was uniform, smooth, and unelastic. Lun and Savage (1987) derived equations for the flow of granular material consisting of monosized, rough spherical particles. Ma and Ahmadi (1990a,b) used a basic mass-weighted averaging technique, and a thermomechanical formulation for multiphase flows was developed. Conservation equations for mass, momentum, and kinetic energy for both phases were obtained. The dissipation rate for gas and solid phase was given as algebraic equations. The model should be suitable for both dilute and dense suspensions. They showed that with only the gas phase present, the model is equivalent to the standard two-equation ($k$-$\epsilon$) model of turbulence, and if the interstitial effects are neglected, the equations are equivalent to those developed from the kinetic theory of dense gases.

Sinclair and Jackson (1989) developed a model for fully-developed gas-solid flow based on the kinetic theory, and with this model they simulated the flow in a small pipe (3 cm). The model was able to account for marked segregation effects of gas and solids in the radial direction and revealed a variety of behavior over the whole range of possible flow conditions.

Based on the work of Jenkins and Savage (1983) and Lun et al. (1984), Ding and Gidaspow (1990) extended their approach from granular flow to gas-solid flow starting with the Boltzmann integral-differential equations for the velocity distribution of the particles. The particles are monosized, smooth and inelastic, and the principal collisional transport consists of binary collision of equal mass particles. The Maxwellian velocity distribution function is used as a single-particle distribution; hence, the model is restricted to dense gas-solid flow only. Gidaspow (1994) extended the model of Ding and Gidaspow (1990) further to non-Maxwellian velocity distributions and thus made the model valid for both dense and dilute gas particle flow by simply adding the respective dense and dilute viscosities and conductivities together. Hjertager and Samuelsberg (1992) and Samuelsberg and Hjertager (1996) have used the kinetic theory and compared predicted time mean and turbulent velocity against data obtained by laser doppler anemometry (LDA).

### *Objectives*

This article presents a verification of an isothermal two-phase two-dimensional gas particle flow model. In the solid phase, a turbulent model is incorporated which is based on kinetic theory description. The model is verified against experimental data from a pilot-scale circulating fluidized-bed reactor with different solid loading and gas superficial velocities by Miller and Gidaspow (1992).

## Fluid Dynamic Model

The governing equations for each phase, together with the constitutive relations, are given in Table 1. The laws of conservation of mass and momentum are satisfied by each phase individually. For the solid phase, the constitutive equations come from the interactions of the fluctuating and the mean motions of the particles. These interactions give rise to an effective shear viscosity for the solid phase, which relates the random motion to the mean motion of the particles. In order to predict these random fluctuations of the solid phase, a turbulent kinetic energy equation is derived for the solid phase. A complete derivation of the governing equations can be found in Gidaspow (1994). The subgrid scale (SGS) model used for the gas phase is taken from Deardorff (1971). Solution of the set of partial differential equations is performed by finite domain methods, and the calculation procedure is taken from the work of Spalding (1985). A full account of the model is given in Samuelsberg (1994).

## Simulation Results

### *Experimental setup*

Miller and Gidaspow (1992) have studied the hydrodynamics of gas/solid flow in the riser part of a circulating fluidized-bed (CFB) reactor. They obtained radial profile data at three different heights in the riser. The X-ray densitometer was used to measure particle concentrations and fluxes were measured by an extraction probe. The riser is 6.6 m high with an ID of 0.075 m. The particles have a mean diameter of $75\times10^{-6}$ m. All measurements were done at heights of 1.86, 4.18, and 5.52 m above the riser inlet. Three different flow conditions were compared with simulations. The solid mass fluxes used are 12.0 and 20.4 kg/m$^2\cdot$s with gas superficial velocities of 2.61, 2.89 and 3.48 m/s.

### *Initial and boundary conditions*

The IIT CFB is simulated in a two-dimensional Cartesian grid. The grid is uniform in the axial direction and is expanded in the radial direction in order to be able to resolve the volume fractions close to the wall. $32\times136$ grid nodes are used to cover the calculation area. The finite difference grid

**Table 1. Kinetic Theory Model for Gas/Solid Flow**

***Continuity Equations***

Gas Phase

$$\frac{\partial(\alpha\rho)_g}{\partial t}+\frac{\partial(\alpha\rho U_i)_g}{\partial x_i}=0$$

Solid Phase

$$\frac{\partial(\alpha\rho)_s}{\partial t}+\frac{\partial(\alpha\rho U_i)_s}{\partial x_i}=0$$

***Momentum Equations***

Gas-Phase Momentum Balance

$$\frac{\partial(\alpha\rho U_j)_g}{\partial t}+\frac{\partial(\alpha\rho U_i U_j)_g}{\partial x_i}=-\alpha_g\frac{\partial P}{\partial x_j}+\alpha_g\rho_g g_j+\frac{\partial\tau_{i,j}}{\partial x_i}+\beta_j(\mathrm{U_{j,s}}-\mathrm{U_{j,g}})$$

Gas-Phase Shear Stress

$$\tau_{i,j}=\mu_g\left[\left(\frac{\partial U_j}{\partial x_i}+\frac{\partial U_i}{\partial x_j}\right)-\frac{2}{3}\delta_{i,j}\frac{\partial U_k}{\partial x_k}\right]$$

SGS Model for Gas-Phase Turbulent Shear Viscosity

$$\mu_g=\mu_l+\mu_t=\mu_l+\rho_g(c_t\Delta)^2(\tau_{i,j}\cdot\tau_{i,j})$$

with $c_t=0.1$ and $\Delta=\sqrt{\Delta x\Delta y}$

Solid-Phase Momentum Balance

$$\frac{\partial(\alpha\rho U_j)_s}{\partial t}+\frac{\partial(\alpha\rho U_i U_j)_s}{\partial x_i}=-\alpha_s\frac{\partial P}{\partial x_j}+\alpha_s\rho_s g_j+\frac{\partial}{\partial x_i}\Pi_{i,j}+\beta_j(U_{j,g}-U_{j,s})$$

Solid-Phase Shear Stress

$$\Pi_{i,j}=-P_s\delta_{ij}+\xi_s\delta_{ij}\frac{\partial U_k}{\partial x_k}+\mu_s\left[\left(\frac{\partial U_j}{\partial x_i}+\frac{\partial U_i}{\partial x_j}\right)-\frac{2}{3}\delta_{ij}\frac{\partial U_k}{\partial x_k}\right]$$

Solids-Phase Pressure

$$P_s=\alpha_s\rho_s[1+2(1+e)\alpha_s g_0]\Theta$$

Radial Distribution Function

$$g_0=\frac{3}{5}\left[1-\left(\frac{\alpha_s}{\alpha_{s,\max}}\right)^{\frac{1}{3}}\right]^{-1}$$

Solid Phase Bulk Viscosity

$$\xi_s=\frac{4}{3}\alpha_s^2\rho_s d_p g_0(1+e)\sqrt{\frac{\Theta}{\pi}}$$

Solid Phase Shear Viscosity

$$\mu_s=\frac{2\mu_{s,\mathrm{dil}}}{(1+e)g_0}\left[1+\frac{4}{5}(1+e)g_0\alpha_s\right]^2+\frac{4}{5}\alpha_s^2\rho_s d_p g_0(1+e)\sqrt{\frac{\Theta}{\pi}}$$

$$\mu_{s,\mathrm{dil}}=\frac{5}{96}\rho_s d_p\sqrt{\pi\Theta}$$

Gas-Solid Drag

$\alpha_s<0.8$

$$\beta=150\frac{\alpha_s^2\mu_g}{\alpha_g(d_p\phi_s)^2}+1.75\frac{\alpha_s\rho_g|\vec{U}_g-\vec{U}_s|}{d_p\phi_s}$$

$\alpha_s\geq 0.8$

$$\beta=\frac{3}{4}C_d\frac{|\vec{U}_g-\vec{U}_s|\rho_g\alpha_s}{d_p\phi_s}\alpha_g^{-2.65}$$

where

$$C_d=\frac{24}{Re}(1+0.15Re^{0.687})\quad\text{for}\quad Re\leq 1{,}000$$

$$C_d=0.44\quad\text{for}\quad Re>1{,}000$$

$$Re=\frac{|\vec{U}_g-\vec{U}_s|\alpha_g\rho_g d_p\Phi_s}{\mu_{l,g}}$$

***Turbulent Kinetic Energy***

$$\frac{3}{2}\left[\frac{\partial}{\partial t}(\alpha\rho\Theta)_s+\frac{\partial}{\partial x_l}(\alpha\rho U_l\Theta)_s\right]=\Pi_{i,j}\frac{\partial U_{j,s}}{\partial x_i}-\frac{\partial}{\partial x_i}\left[\Gamma_\Theta\frac{\partial\Theta}{\partial x_i}\right]-\gamma$$

Collisional Energy Dissipation

$$\gamma=3(1-e^2)\alpha_s^2\rho_s g_0\Theta\left[\frac{4}{d_p}\sqrt{\frac{\Theta}{\pi}}-\frac{\partial U_{k,s}}{\partial x_k}\right]$$

Transport Coefficient of Turbulent Kinetic Energy

$$\Gamma_\theta=\frac{2\Gamma_{\Theta,\mathrm{dil}}}{(1+e)g_0}\left[1+\frac{6}{5}(1+e)g_0\alpha_s\right]^2+2\alpha_s^2\rho_s d_p g_0(1+e)\sqrt{\frac{\Theta}{\pi}}$$

$$\Gamma_{\Theta,\mathrm{dil}}=\frac{75}{384}\rho_s d_p\sqrt{\pi\Theta}$$

is shown in Figure 1. Uniform one-dimensional plug flow is assumed at the inlet boundary, where velocities and volume fractions are specified for both phases. A constant inlet particle volume fraction of 0.1, a constant inlet particle inlet velocity deduced from a prescribed solids mass flux and zero inlet granular temperature are used in all simulations. The coefficient of restitution, $e$, was taken to be 0.995. The outlet boundary is at the right side of the calculation domain as shown in Figure 1. A continuation condition for all dependent variables is assumed for both phases at the outlet boundary. At the walls, a no-slip condition is imposed for the gas velocity; a free slip velocity is used for the particle velocity and zero gradient is used for the granular temperature. An empty pipe at ambient temperature is used as an initial start condition. All simulations are continued for 50 s of real simulation time which was sufficient to obtain a statistically stationary flow. In order to get reasonable time-averaged results to compare against the experiments, the time average is taken from the last 20 s of the simulations.

### *Particle velocity profiles*

Miller and Gidaspow (1992) obtained solid velocity profiles indirectly from the solid flux and volume fraction profiles via the algebraic relation

$$v_p=\frac{G_p}{\alpha_p\rho_p}\tag{1}$$

In Figures 2, 3 and 4 the simulated and experimental axial solid velocity profiles are plotted for a solid mass flux of 20.4

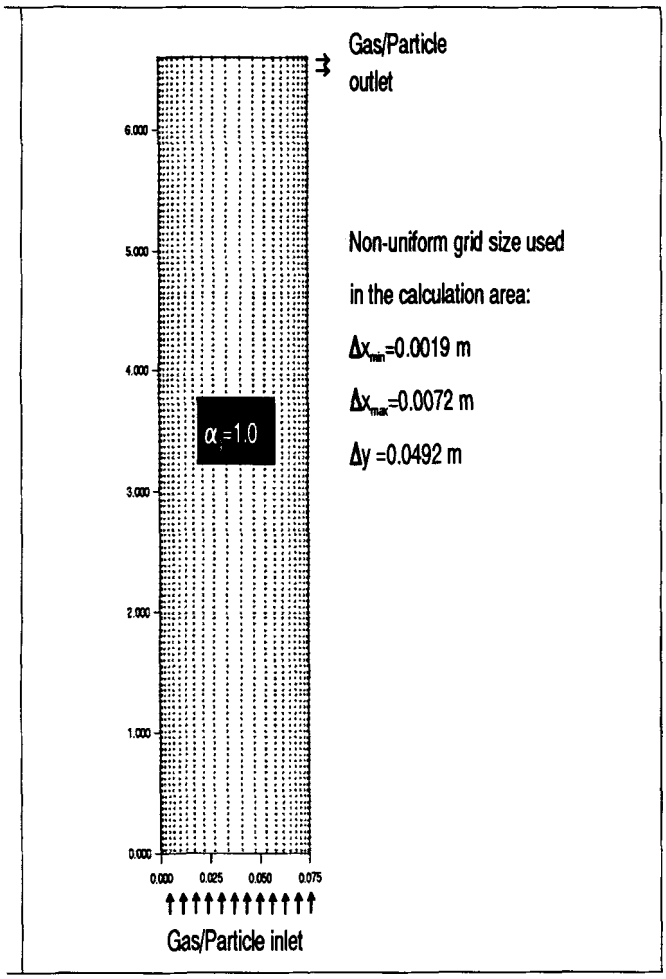


**Figure 1. Finite volume grid used for the simulations.**

kg/m$^2$·s and gas superficial velocity of 2.61, 2.89 and 3.48 m/s, respectively.

At 1.86 m above the inlet, the core velocity is highest for the highest gas superficial velocity. This is consistent with the experimental results. All cases fit with the experimental results although the maximum velocity for the case with gas superficial velocity of 2.89 m/s is somewhat overpredicted, which therefore underestimates the core size. When the height is 4.18 m above the inlet, the trend is the same. There is a slight acceleration in all cases, but the highest gas superficial velocity still has the highest core velocity in the simulations. The experiments give a uniform velocity profile with almost no downflow close to the wall, and with highest core velocity when the gas superficial velocity is 2.89 m/s. When the gas superficial velocity is raised to 3.48 m/s, no backflow of particles is measured as shown in Figure 4. Due to this, the core diameter expands and thereby the core velocity decreases. This trend is not captured in the simulation.

At 5.52 m, the experimental profiles change form. The velocity profiles are smoother and the radius of the core has increased. This is due to a retardation in core velocity. The maximum velocity has almost the same value in all cases, but is lower than for the level at 4.18 m. The simulations gave a sharper bell-shaped velocity profile, but with the correct magnitude in the core. Due to this, the downflow close to the wall is overpredicted in all simulations.

### *Radial solid volume fraction profiles*

Figures 5 and 6 show simulated and experimental solid volume fraction profiles for cases with gas superficial velocity of 2.89 m/s and solid flux of 12.0 kg/m$^2$·s, and gas superficial velocity of 2.61 m/s and solid flux of 20.4 kg/m$^2$·s.

At 1.86 m above the inlet, Miller and Gidaspow (1992) reported that the riser is closely packed in a bubbling flow situation. Because of the different inlet situations between the experimental and the simulated situation, there is reason to believe that it will not be possible to correctly predict the volume fractions at the lowest sections with the chosen inlet condition. However, still, the simulations give a dilute core and a denser annulus, even if the level especially for the most dense case is far to low in Figure 5. This is not surprising, since the difference will grow with increasing solid feed flux.

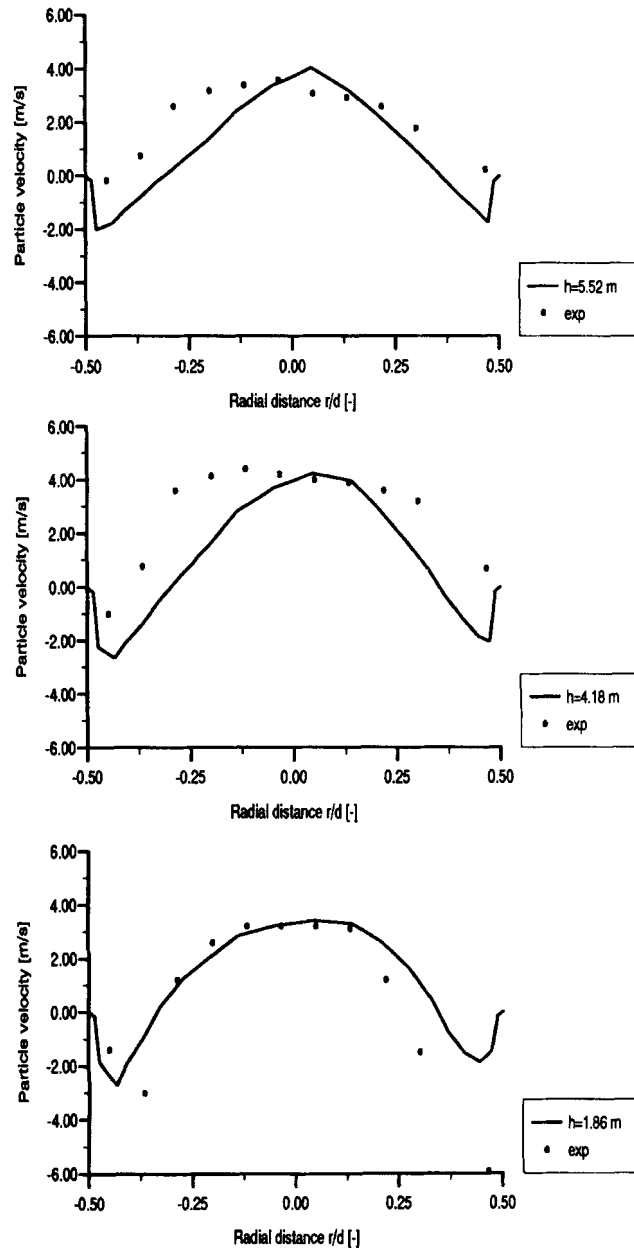


**Figure 2. Solid velocity profiles.**

$V_{g,sup}$ = 2.61 m/s.

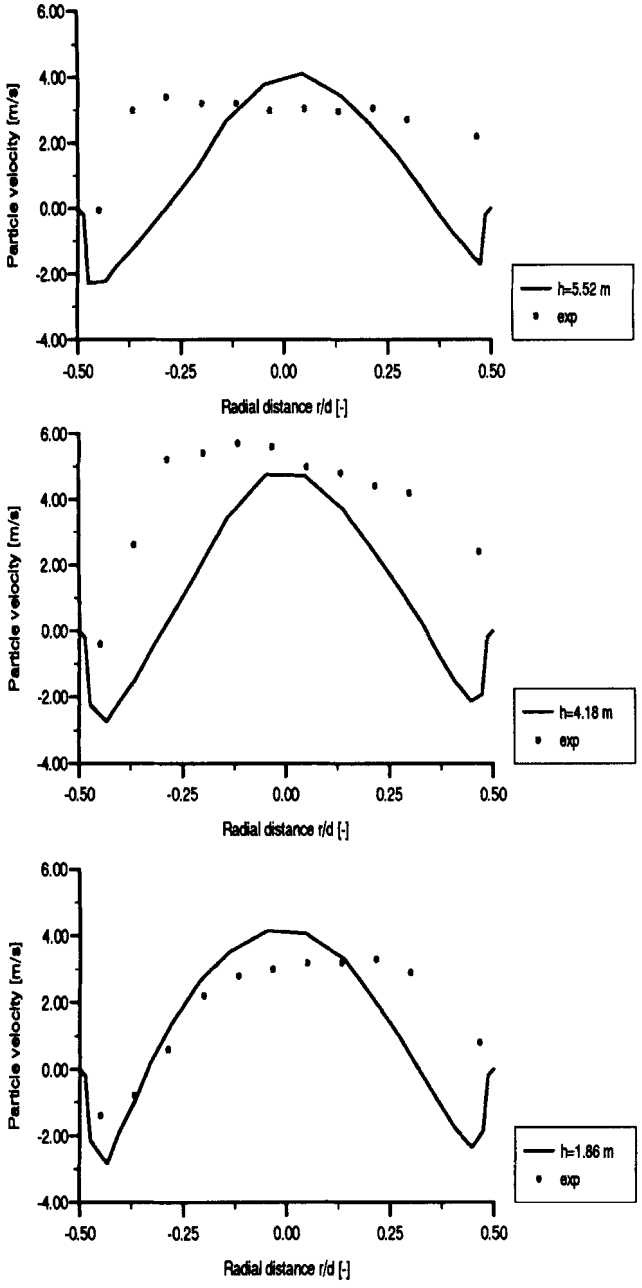


**Figure 3. Solid velocity profiles.**

$V_{g,sup} = 2.89$ m/s.

When the height is 4.18 m, the core and annulus are correctly predicted in Figure 5. The simulated average volume fractions equal the experimental, which is 0.03. In Figure 6, the correct values are predicted in both core and annulus.

At 5.52 m, the simulated values close to the wall are higher than at 4.18 m in Figure 5. This trend is like the experimental results. The solid volume fraction in the core has the correct level, but is not constant. In Figure 6, again the correct concentrations are predicted in the core and annulus. In the positions closest to the wall, the predicted volume fractions are higher at this level compared to the level 4.18 m. It is evident from Figures 5 and 6, as well as from the solid velocities curves, that the flow is not fully developed in the riser, even with its relatively large length/diameter ratio of 84. The same conclusion is also found in the Miller and Gidaspow (1992) experiment.

### *Axial solid volume fraction profiles*

The different sections in a riser can generally be divided into three distinct zones. Just above the inlet, there is a dense zone with approximately constant volume fraction. This section can be looked upon as a dense turbulent bubbling bed. Then comes a freeboard zone with an often slight decrease in volume fraction with increasing height, and at the top of the riser an exit zone with a slight increase/decrease in solid volume fraction depending on the outlet geometry. The increase in volume fraction is in this simulation, due to the 90° bend at the outlet boundary.

Figure 7 shows the radially average solid volume fraction as a function of the riser height for three different gas super-

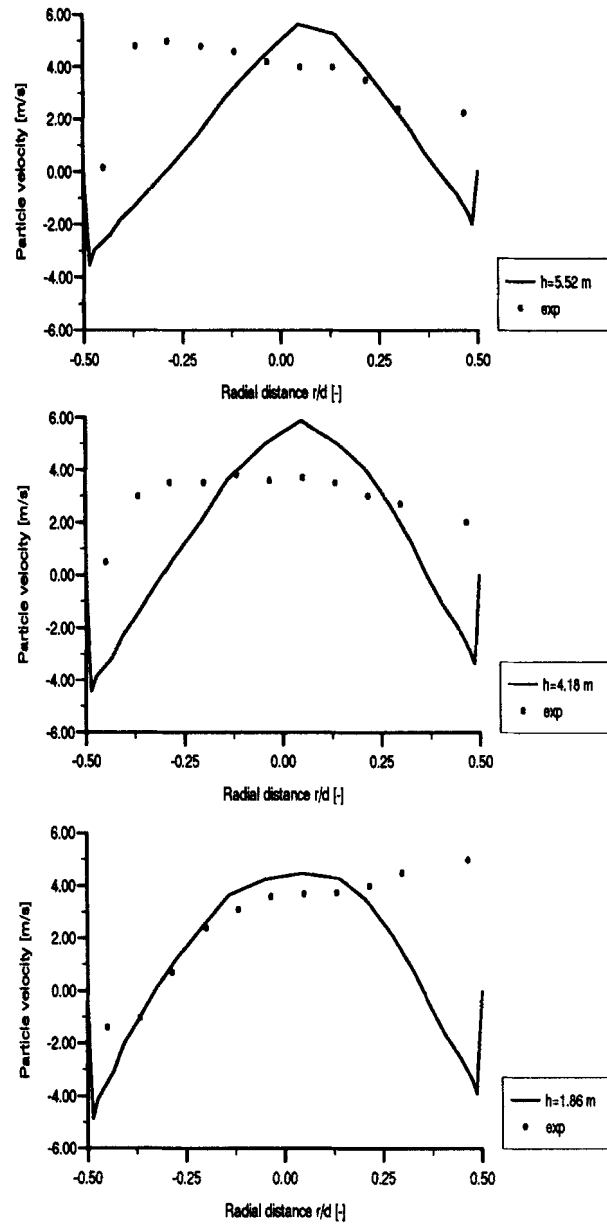


**Figure 4. Solid velocity profiles.**

$V_{g,sup} = 3.48$ m/s.

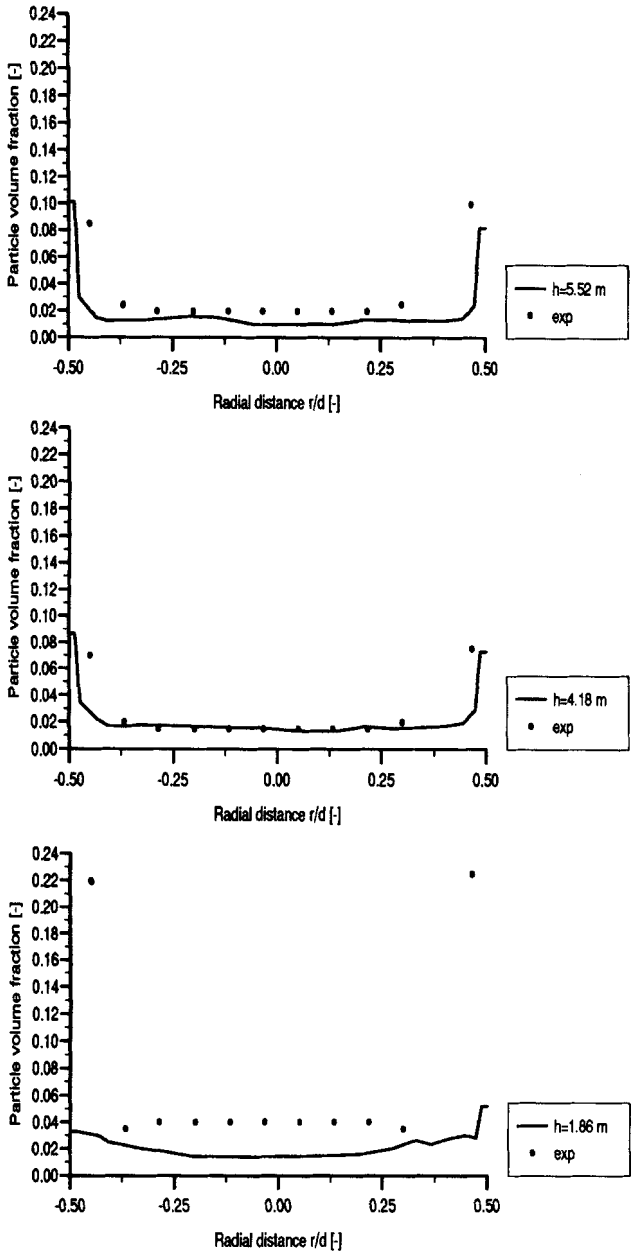


**Figure 5. Experimental and simulated solid volume fraction profiles.**

$V_{g,\mathrm{sup}} = 2.61$ m/s.

ficial velocities and with a solid inlet flux of 20.4 kg/m$^2$s. In the dense section all profiles have the same uneven distribution with a volume fraction somewhat higher than the volume fraction in the freeboard zone. This dense region extends approximately 1 m above the inlet. In the freeboard section, the profiles exhibit a different shape. The simulations with the two lowest gas superficial velocities have the same trend with a slight decrease in volume fraction the first meter. A 2-m section with increasing volume fraction has constant volume fraction, whereas the last meter has a sharp decrease followed by a corresponding sharp increase afterward.

The highest gas superficial velocity gives a different profile in the freeboard. This profile decreases evenly all the way until it reaches the exit zone where it increases sharply at the same height just as the other profiles.

In Figures 8, 9 and 10, the axial time averaged variation of solid volume fraction, for the same conditions as in Figure 7, is shown for three different radial positions, left, middle and right in the riser respectively. In Figures 8 and 10, left and right in the riser, there is a relatively dense section in the first meter above the distributor. In Figure 9, the cases with highest and lowest superficial gas velocity have the highest volume fraction, while in Figure 10 there is no such distinct difference. In the core, Figure 9 shows a relatively denser bed when the superficial gas velocity is raised to 3.48 m/s.

In all cases, the transition from dense to dilute bed starts at the same height. This transition starts approximately 0.7 m

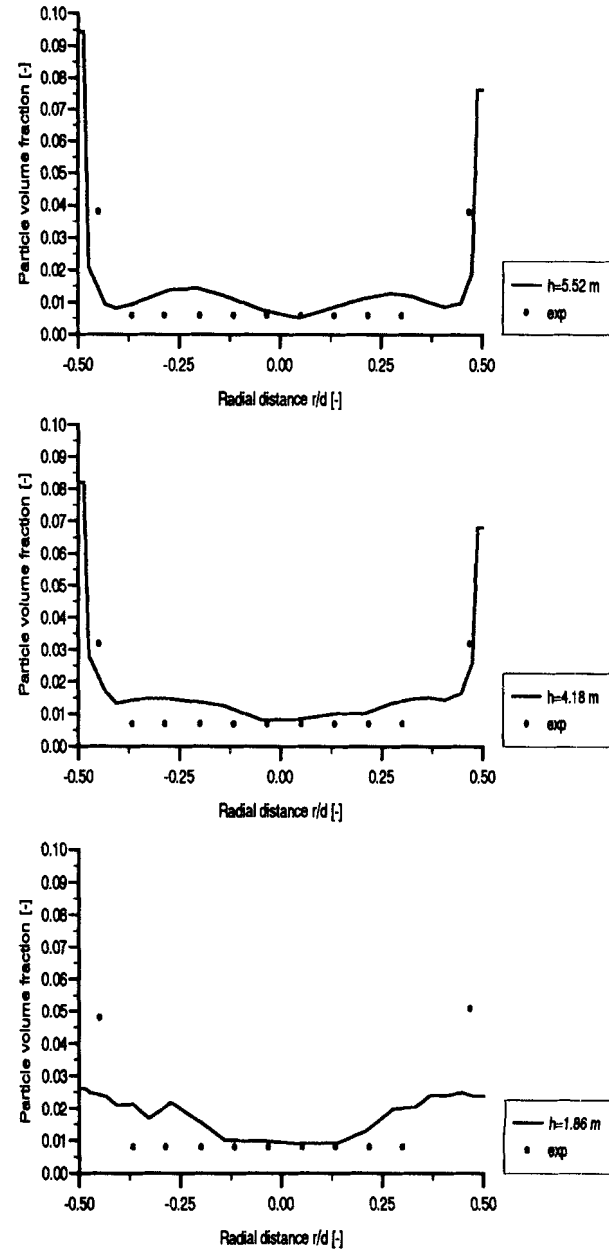


**Figure 6. Experimental and simulated solid volume fraction profiles.**

$V_{g,\mathrm{sup}} = 2.89$ m/s.

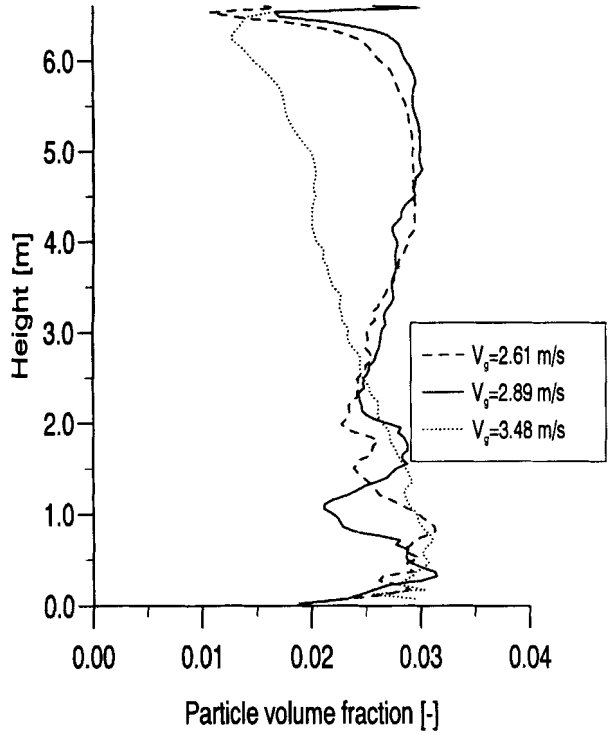


**Figure 7. Axial variation of radial averaged solid volume fraction.**

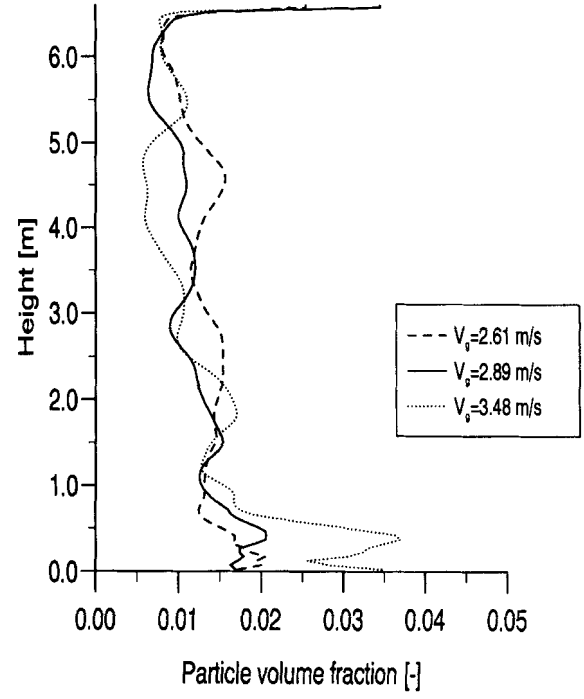


**Figure 9. Axial variation of solid volume fraction in the center of the riser.**

above the inlet. From 1 to 6 m above the inlet boundary the solid volume fraction is almost independent of the height and radial position, except for the case with gas superficial velocity of 3.48 m/s in the annulus. With this velocity, the volume fractions of solids are decreasing steadily, as shown in Figures 8 and 10. In the last 0.6 m of the riser, the volume fraction decreases strongly on the left side as expected, whereas the profiles in the middle and close to the left outlet in the riser have a sharp increase in volume fraction. In Figure 11 this is indicated by plotting the particle flow pattern after 46

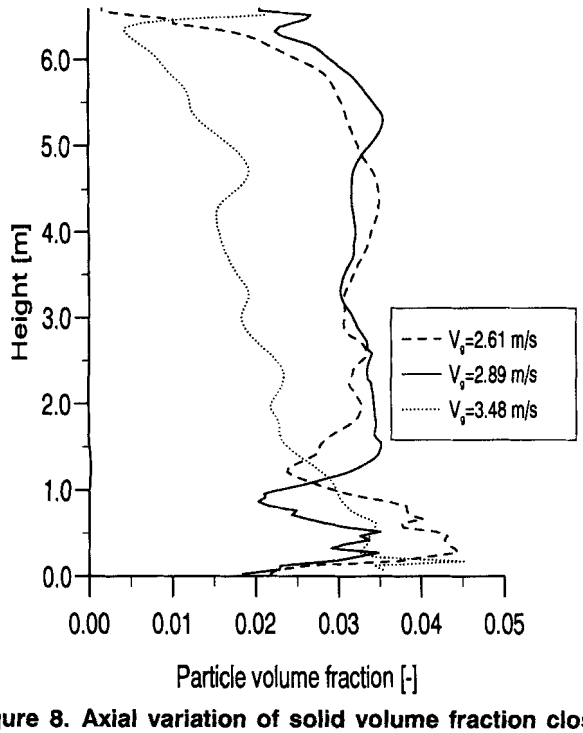


**Figure 8. Axial variation of solid volume fraction close to the left wall.**

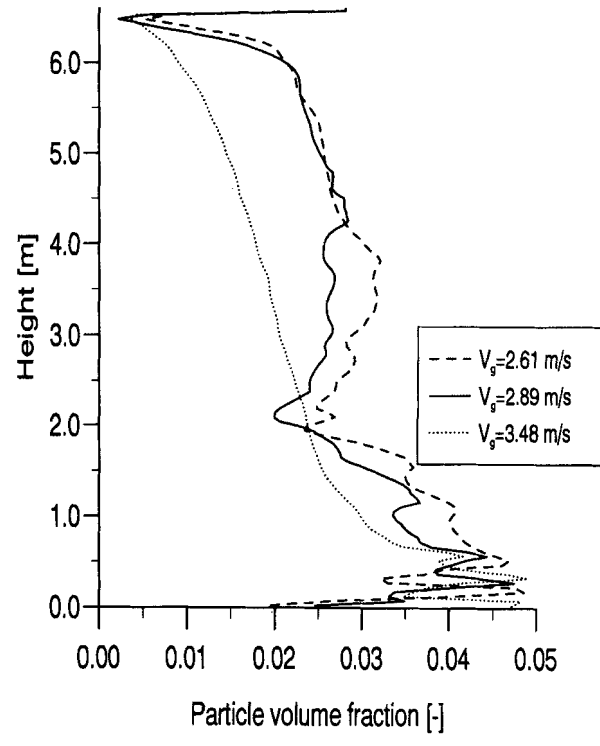


**Figure 10. Axial variation of solid volume fraction close to the right wall.**

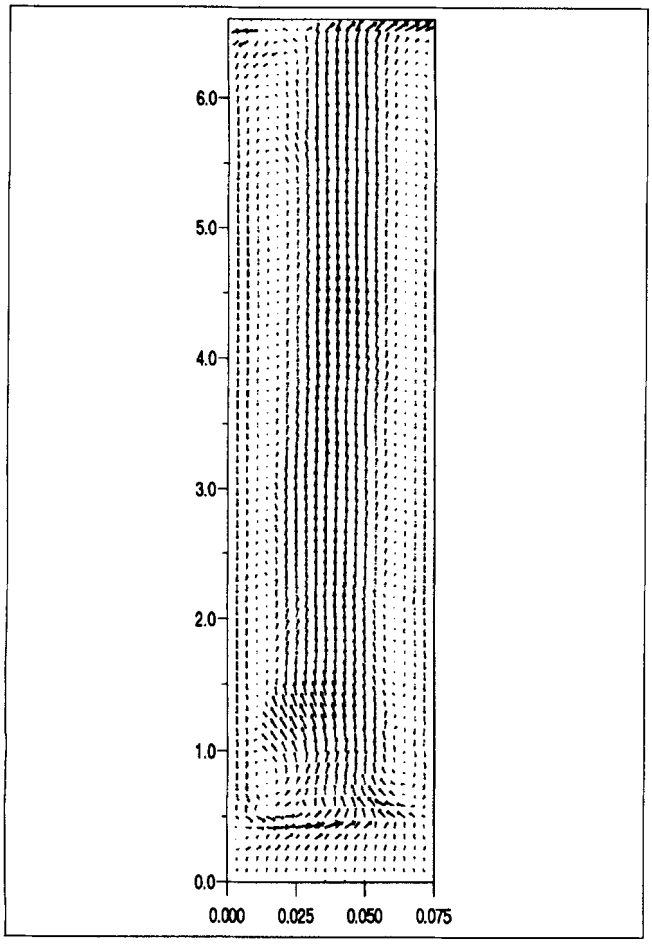


**Figure 11. Solid phase vector plot after 46 s of real simulation time.**

s for the case with gas superficial velocity of 2.89 m/s. Here, a central core with gas and particles moving upwards with backmixing and downflow along both walls can be seen. For the largest particle fraction gradients in Figures 8 and 10, radial mixing between the core and annulus takes place. This is consistent with Figure 11 where the solid flow direction turns. In the lower part, the particle moves from the wall towards the center and in the upper part, the particle direction is reversed.

### *Outlet particle flux*

Although the inlet boundary conditions are steady, the flow never reaches a steady state. The gas and the solid will oscillate with a frequency that varies with gas superficial velocity and solid flux. These oscillations increase with increasing riser height and increasing feed flux and will reach a maximum at the top of the riser due to less dampening effect in the upper part. Figures 12, 13 and 14 show the solid mass flux oscillation at the outflowing boundary for the case with particle feed flux of 20.4 kg/m$^2$·s and gas superficial velocity of 2.61, 2.89 and 3.48 m/s. The slugs that could be observed visually are also predicted in the simulations. The mean flux of these slugs can grow to more than three times the inlet mass flux.

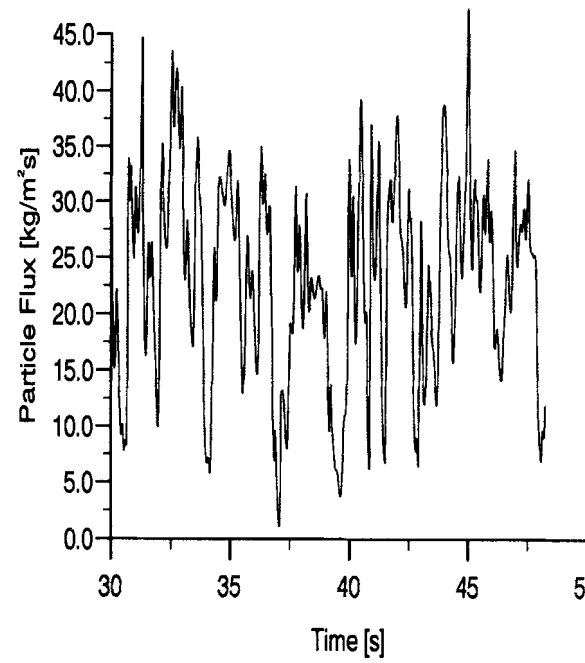


**Figure 12. Outlet particle flux.**
$V_{g,sup}$ = 2.61 m/s.

### *Particles shear viscosity*

In fluidized beds, solids viscosity plays a major role. Inviscid models are not able to predict forces on immersed bodies. It is known that wall effects play an important role in CFBs. Cluster formation and downflow along the walls is not possible to model without a viscosity. This is not the true fluid viscosity, but must be looked upon as being an eddy type viscosity. Earlier attempts to model CFBs had to use a constant estimated value for the viscosity (Tsuo and Gi-

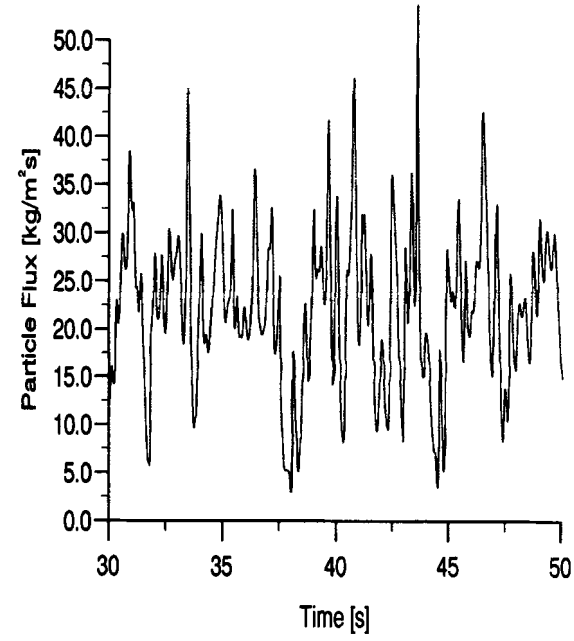


**Figure 13. Outlet particle flux.**
$V_{g,sup}$ = 2.89 m/s.

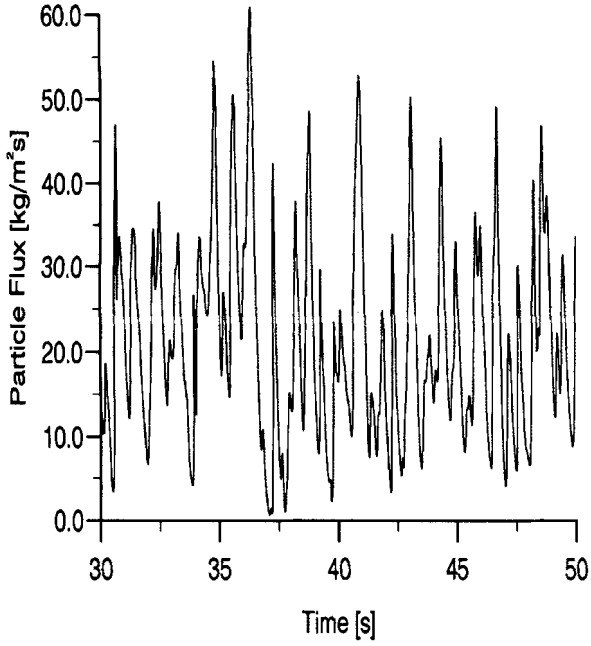


**Figure 14. Output particle flux.**

$V_{g,\text{sup}} = 3.48$ m/s.

daspow, 1990). In the new modeling approach, using methods from kinetic gas theory, the solids shear viscosity is computed.

Miller and Gidaspow (1992) determined the solid viscosity from a mixture momentum balance, neglecting transient effects and assuming that the gas and solid velocity gradient are of the same order. The mixture momentum balance is then written as

$$\frac{\partial(\alpha\rho v^2)_p}{\partial z} = -\frac{\partial P}{\partial z} + \frac{1}{r}\frac{\partial}{\partial r}\left(r\mu_p\frac{\partial v_p}{\partial r}\right) - \alpha_p\rho_p g \qquad (2)$$

After integration, algebraic manipulation and assuming that the solid velocity gradients are symmetric across the riser diameter and that the pressure is a negligible function of the radial position, Miller found the mixture momentum balance to be

$$\frac{2}{R^2}\int_0^R \frac{\partial(\alpha\rho v^2)_p}{\partial z} r dr - \frac{2}{R}\mu_p\frac{\partial v_p}{\partial r}\bigg|_{r=R} = -\frac{\partial P}{\partial z} - \int_0^R \alpha_p\rho_p g r dr \qquad (3)$$

This equation states that the pressure drop minus the weight of the bed is equal to the shear plus the axial acceleration for any position that Miller and Gidaspow (1992) evaluated the shear rate as the derivative of the velocity profile with respect to radial position. The axial acceleration and the weight of the bed were determined directly from integration of the solid volume fraction, velocity, and flux profiles. From Eq. 3, they found that the solid viscosity can be approximated by the solid volume fraction multiplied by a constant

$$\mu_p = 0.535 \cdot \alpha_p \quad [\text{Pa}\cdot\text{s}] \qquad (4)$$

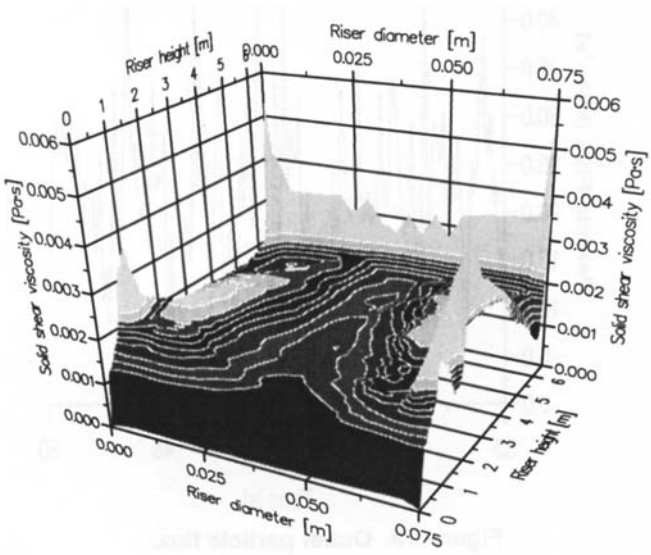


**Figure 15. Computed time-averaged shear viscosity.**

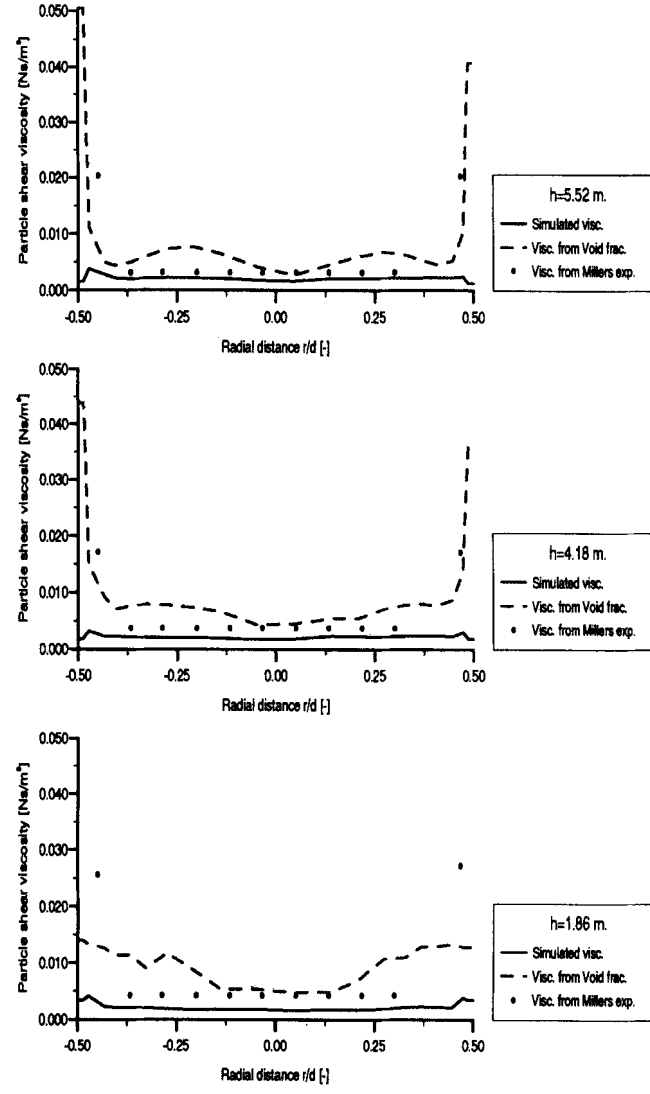


**Figure 16. Solids shear viscosity profiles.**

$G_s = 12.0$ kg/m$^2$·s; $V_{g,\text{sup}} = 2.89$ m/s.

In Figure 15, the time-averaged solid shear viscosity calculated according to the expression in Table 1 is plotted for the case with superficial gas velocity of 2.89 m/s and solid mass flux of 20.4 kg/m$^2$·s. The computed solids shear viscosities are between 0.001 and 0.006 Pa·s. The shear viscosity is mainly due to high velocity gradients. In the inlet zone, the particles accelerate and the shear viscosity is very low. In the core the shear viscosity increases slightly with riser height, whereas in the annulus there are higher velocity gradients, so viscosity increases towards the wall. The highest viscosity is found in the transition from dense to dilute bed and at the top of the riser where the particles have to make a turn back to the bed. There is also a sharp decrease of viscosity close to the outlet at the right side of the riser. The time-averaged radial profile for the case with superficial gas velocity of 2.89 and 2.61 m/s, and solid mass fluxes of 12.0 and 20.4 kg/m$^2$·s are shown in Figures 16 and 17, respectively. In these figures, the computed viscosity from kinetic theory using the equation given in Table 1 and the viscosity predicted from Eq. 4 using both computed and measured solid volume fraction are shown. In Figure 16, all profiles except at the lowest level lie within the same order of magnitude in the core. In the annulus, however, the computed viscosity from kinetic theory is not able to reproduce the predicted velocity from Eq. 4. In Figure 17, the computed viscosity from kinetic theory is in the same order of magnitude as in Figure 16; however, here the other profiles in the core are one order of magnitude higher.

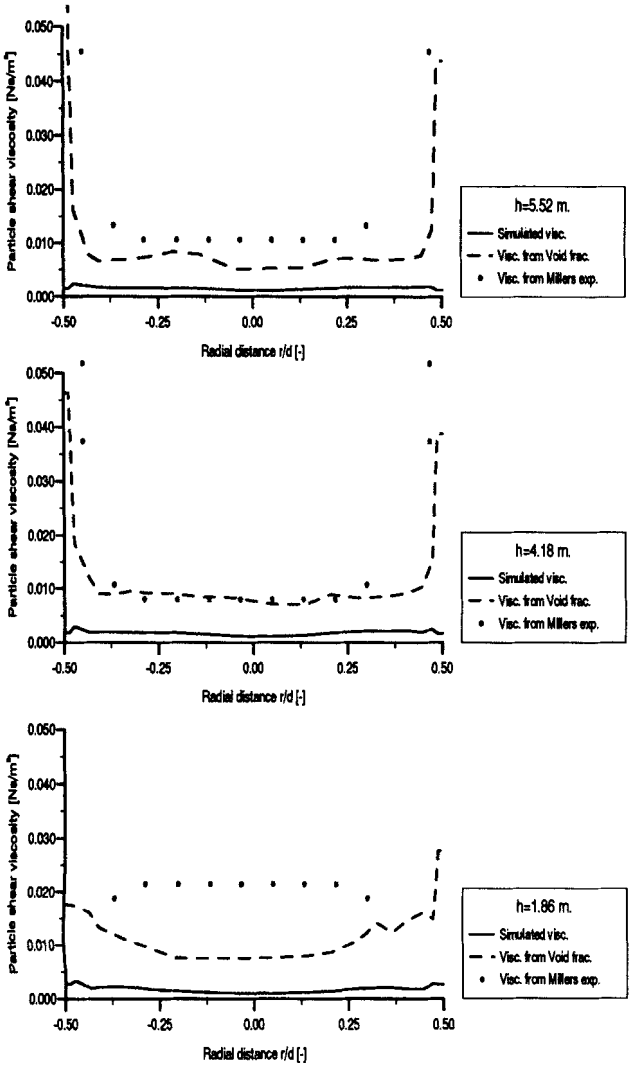


**Figure 17. Solids shear viscosity profiles.**

$G_s$ = 20.4 kg/m$^2$·s; $V_{g,\text{sup}}$ = 2.61 m/s.

## Conclusions

The gas/particle flow model is compared against experimental solids velocity and volume fraction data obtained in a CFB. In the experiments, both the solids loading and gas superficial velocity were varied. Generally, the riser is divided into two zones, with a dense bubbling zone in the bottom section and a dilute core in the upper part. Internal backmixing of gas and solids can be observed. The flow model is able to predict core annulus flow during the various conditions. The predicted velocities show good agreement with the measurements in both the core and annulus for all the test cases. The computed solid volume fraction agrees well with the experimental data, except for the level closest to the inlet boundary. This may be due to the difference in the inlet geometry description. The discrepancies between experimental and predicted results may be due to the difference in the way the gas and solids are described at the in- and outflowing boundaries. Only the riser part of the CFB is simulated. In addition to this simplification at the inlet a one-dimensional plug flow is prescribed and at the outlet a 90° bend is used.


## Acknowledgment

This work is financially supported by Norsk Hydro a.s, Research Centre, and the Research Council of Norway through the State R&D Programme for Utilization of Natural Gas (SPUNG) program.


## Notation

$C_d$ = drag coefficient
$C_t$ = constant in effective gas-phase viscosity
$d_p$ = particle diameter
$e$ = coefficient of restitution
$G_s$ = solid mass flux
$g_j$ = $j$-direction component of gravity
$g_0$ = radial distribution function
$p$ = pressure
$r$ = radius
$R$ = inner radius of riser
$Re$ = Reynolds number
$t$ = time
$u$ = $x$-direction velocity
$U_i, U_j$ = $i$ and $j$ components of velocity for gas and solid
$\vec{U}_g, \vec{U}_p$ = gas and solids velocity vector
$v$ = $y$-direction velocity
$x_j$ = coordinate direction in the $j$ direction
$x$ = coordinate in the $x$ direction
$y$ = coordinate in the $y$ direction
$z$ = height coordinate

### *Greek letters*

$\alpha$ = volume fraction
$\beta$ = two-phase drag coefficient
$\gamma$ = collisional energy dissipation
$\Gamma$ = transport coefficient
$\delta_{ij}$ = Kronecker delta
$\Delta t$ = time step
$\Delta x$ = $x$-direction width of the control-volume
$\Delta y$ = $y$-direction width of the control-volume

$\theta$ = granular temperature or 2/3 times the turbulent kinetic energy of particles
$\kappa$ = thermal conductivity
$\mu$ = shear viscosity
$\xi$ = solid bulk viscosity
$\pi$ = 3.14
$\Phi$ = sphericity of the particles
$\Pi$ = stress tensor solid phase
$\rho$ = density
$\tau$ = stress tensor gas phase

### *Subscripts*

*dil* = dilute
$g$ = gas phase
$ij$ = vector component of $ij$
$i$ = vector component of $i$
$j$ = vector component of $j$
$k$ = vector component of $k$
$p$ = particle phase
$s$ = solids
sup = supercritical

## Literature Cited


Chapman, S., and T. G. Cowling, *The Mathematical Theory of Non-Uniform Gases*, 3rd ed., Cambridge Univ. Press (1970).

Deardorff, J. W., "On the Magnitude of the Sub Grid Scale Eddy Coefficient," *J. Comput. Phys.*, **7**, 120 (1971).

Ding, J., and D. Gidaspow, "Bubbling Fluidization Model Using Kinetic Theory of Granular Flow," *AIChE J.*, **36**(4), 523 (1990).

Ding, J., and R. W. Lyczkowski, "Three-Dimensional Kinetic Theory Modelling of Hydrodynamics and Erosion in Fluidized Beds," *Powder Technol.*, **73**, 127 (1992).

Gidaspow, D., "Hydrodynamics of Fluidization and Heat Transfer: Supercomputer Modelling," *Appl. Mech. Rev.*, **39**(1), 1 (1986).

Gidaspow, D., Y. P. Tsuo, and K. M. Luo, "Computed and Experimental Cluster Formation and Velocity Profiles in Circulating Fluidized Beds," *Circulating Fluidized Beds: Fluidization IV*, Int. Fluidization Conf., Banff, Alberta, Canada (1989).

Gidaspow, D., *Multiphase Flow and Fluidization—Continuum and Kinetic Theory Descriptions*, Academic Press, New York (1994).

Harris, B. J., and J. F. Davidson, "Modelling Options for Circulating Fluidized Beds: A Core/Annulus Deposition Model," Int. Conf. on Circulating Fluid Beds, p. 35 (1993).

Hjertager, B. H., and A. Samuelsberg, "Computational Simulation of Flow Processes in Fluidized Bed Reactors," *KONA Powder and Particle*, **10**, 96 (1992).

Jenkins, J. T., and S. B. Savage, "A Theory for the Rapid Flow of Identical, Smooth, Nearly Elastic, Spherical Particles," *J. Fluid Mech.*, **130**, 187 (1983).

Kostamis, P., C. W. Richards, and N. C. Markatos, "Numerical Simulation of Two-Phase Flows with Chemical Reaction and Radiation," *PhysicoChem. Hydrody.*, **9**, 219 (1987).

Kuipers, J. A. M., "A Two-Fluid Micro Balance Model of Fluidized Beds," PhD Diss., Twente Univ. of Technology, The Netherlands (1990).

Kuipers, J. A. M., K. J. van Duin, F. P. H. van Beckum, and W. P. M. van Swaaij, "A Numerical Model of Gas-Fluidized Beds," *Chem. Eng. Sci.*, **47**(8), 1913 (1992).

Kuipers, J. A. M., H. Tammes, and W. P. M. van Swaaij, "Experimental and Theoretical Porosity Profiles in a Two-Dimensional Gas-Fluidized Bed with a Central Jet," *Powder Technol.*, **71**, 87 (1992).

Lun, C. K. K., S. B. Savage, D. J. Jeffrey, and N. Chepurniy, "Kinetic Theories for Granular Flow: Inelastic Particles in Couette Flow and Slightly Inelastic Particles in a General Flowfield," *J. Fluid Mech.*, **140**, 223 (1984).

Lun, C. K. K., and S. B. Savage, "A Simple Kinetic Theory for Granular Flow of Rough, Inelastic Spherical Particles," *J. Applied Mech.*, **57**, 47 (1987).

Lyczkowski, R. W., S. Folga, S. L. Chang, J. X. Bouillard, C. S. Wang, G. F. Berry, and D. Gidaspow, "State-of-the-Art Computation of Dynamics and Erosion in Fluidized Bed Tube Banks," *Can. Chem. Eng.*, **67**, 465 (1989).

Ma, D., and G. Ahmadi, "A Thermodynamical Formulation for Dispersed Multiphase Turbulent Flows—I," *Int. J. Multiphase Flows*, **16**(2), 323 (1990a).

Ma, D., and G. Ahmadi, "A Thermodynamical Formulation for Dispersed Multiphase Turbulent Flows—II," *Int. J. Multiphase Flows*, **16**(2), 341 (1990b).

Miller, A., and D. Gidaspow, "Dense, Vertical Gas-Solid Flow in a Pipe," *AIChE J.*, **38**(11), 1801 (1992).

Samuelsberg, A., "Modelling and Simulation of Fluidized Bed Reactors," Dr.Ing. Thesis, Telemark Inst. of Technology, Porsgrunn, Norway (1994).

Samuelsberg, A., and B. H. Hjertager, "An Experimental and Numerical Study of Flow Patterns in a Circulating Fluidized Bed Reactor," *Int. J. Multiphase Flows*, in press (1996).

Samuelsberg, A., and B. H. Hjertager, "Simulation of Two-Phase Gas/Particle Flow and Ozone Decomposition in a 0.25 I. D. Riser," *Int. Conf. on Multiphase Flow*, Kyoto, Japan (Apr. 3–7, 1995).

Spalding, D. B., "Computer Simulation of Two-Phase Flows with Special Reference to Nuclear Reactor Systems," *Computational Techniques in Heat Transfer*, R. W. Lewis, K. Morgan, J. A. Johnsen, and W. R. Smith, eds., Pineridge Press, p. 1 (1985).

Theologos, K. N., and N. C. Markatos, "Modelling of Flow and Heat Transfer in Fluidized Catalytic Cracking Riser-Type Reactors," *Trans. IChemE.*, **70**, Part A, 239 (1992).

Theologos, K. N., and N. C. Markatos, "Advanced Modelling of Fluid Catalytic Cracking Riser-Type Reactors," *AIChE J.*, **39**(6), 1007 (1993).

Tsuo, Y. P., and D. Gidaspow, "Computation of Flow Patterns in Circulating Fluidized Beds," *AIChE J.*, **36**(6), 885 (1990).


*Manuscript received Dec. 27, 1994, and revision received July 21, 1995.*